JOURNAL OF MATERIALS SCIENCE 14 (1979) 1192–1206

Anisotropic properties of unidirectionally crystallized calcium metasilicate

P. S. ROGERS, R. M. WESTON
Department of Metallurgy and Materials Science, Imperial College, London, UK

The anisotropy displayed by materials which contain aligned, fibrous crystals in a crystalline or glass matrix has been investigated. The materials were prepared by the unidirectional crystallization of calcium metasilicate from glasses and melts of approximately metasilicate compositions. Rectangular prism test specimens were fabricated such that the fibre axis ran parallel to the long axis, across the width or through the depth. This enabled the variation of properties with fibre orientation to be established. The high-temperature polymorph, α-$CaSiO_3$, could be crystallized dendritically such that the primary arms were aligned, and the growth of secondary arms inhibited, by mutual impingement. β-$CaSiO_3$, the low-temperature polymorph, has a chain silicate structure and crystallized as fibres by the spherulitic crystallization mechanism. These fibres grew in approximately parallel alignment due to transcrystallization. The glass remaining after crystallization of the primary phase was either stable or subsequently crystallized from nuclei on the primary crystals, giving materials with either a glass or crystalline matrix respectively. Thermal expansion data were obtained from an automatic recording dilatometer, and the moduli of rupture and shear strengths were found using three-point bend tests of appropriate span-to-depth ratios. The results of these tests showed that the unidirectionally crystallized materials behaved similarly to conventional brittle matrix / brittle fibre composites.

1. Introduction

In situ composites are aligned two-phase materials in which the two phases are produced simultaneously by the decomposition of a single-phase starting material. The unidirectional solidification of eutectic melts is the most widely investigated technique for the production of these materials, although in recent years the unidirectional decomposition of eutectoids or supersaturated solid solutions has also been used to produce successful composites. Livingston [1] has reviewed duplex (two-phase) crystal growth as applied to the production of aligned composites. Most research has been on metallic systems, reviewed by Davies [2], but several oxide eutectic systems have also been directionally solidified, e.g. the ZrO_2–MgO eutectic [3]. Recently, Carpay and Cense have developed a method for the production of *in situ* composites by unidirectional crystalline decomposition of non-crystalline solids using quenched salts and oxides [4, 5].

In situ composites may have a rod-like, ribbon-like or lamellar microstructure when produced by the growth of duplex crystals, and the type of morphology depends on the volume fraction of phases at the transformation temperature and the anisotropy of the solid–solid surface energies between these phases. It has been generally found that rod-like *in situ* composites, analogous to conventional unidirectional continuous fibre-reinforced composites, can only be produced with relatively low fibre volume fractions [1]. The physical properties of these composite materials are anisotropic and depend on the properties of the constituent phases and the volume fraction, morphology and alignment of these phases.

Conventional glass-ceramics are polycrystalline solids prepared by the controlled internal

TABLE I Weighed-out compositions of the glasses

Glass	Wt% composition						Mol% composition					
	SiO_2	CaO	Al_2O_3	ZnO	Na_2O	CaF_2	SiO_2	CaO	Al_2O_3	ZnO	Na_2O	CaF_2
I	50.9	29.6	12.0	7.4			53.5	33.3	7.4	5.7		
II	55.0	35.0	5.0		5.0		54.9	37.4	2.9		4.8	
IIR	64.0		17.0		19.0		69.2		10.8		19.9	
IIF	54.7	29.9	4.3		4.3	6.8	55.4	32.5	2.6		4.2	5.3
III	50.0	30.0		20.0			51.2	33.4		15.4		

nucleation and crystallization of a glass. They are, therefore, materials in which there is a random dispersion of one or more crystalline phases, together with a small proportion of residual glass. The macroscopic physical properties of these materials are isotropic [6]. Several attempts have been made to produce anisotropic glass-ceramics [7], and recently both Ashbee [8] and Atkinson and McMillan [9] have developed techniques to orientate glass-ceramic microstructures using hot-extrusion techniques.

During the investigation of the effects of various transition metal oxides on the crystallization of $CaO-MgO-Al_2O_3-SiO_2$ glasses of approximately metasilicate composition, Rogers and co-workers found that for glasses containing vanadium oxides [10] or zinc oxide [11] the crystalline phases nucleated at the external surface of the glass and subsequently grew as thin needles towards the centre of the sample. A more detailed study of the $CaO-Al_2O_3-SiO_2$ system [12], containing either ZnO or Na_2O to increase the devitrification rates, has found two compositions, glasses I and II in Table I, which gave densely surface-nucleated, fibrous crystals of β-$CaSiO_3$ in

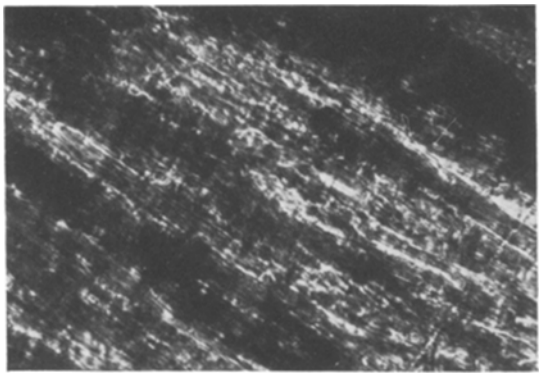

Figure 1 Composition I isothermally crystallized at 1180° C. β-$CaSiO_3$ fibres in a matrix of crystalline $CaAl_2Si_2O_8$ and residual glass (× 500).

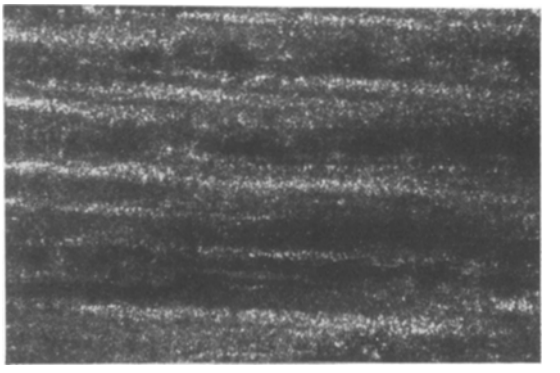

Figure 3 Composition III pulled from a molten zone at 30 μm sec^{-1}, on a composition II β-$CaSiO_3$ "seed" block. β-$CaSiO_3$ fibres in a matrix of $Ca_2ZnSi_2O_7$ and residual glass (× 500).

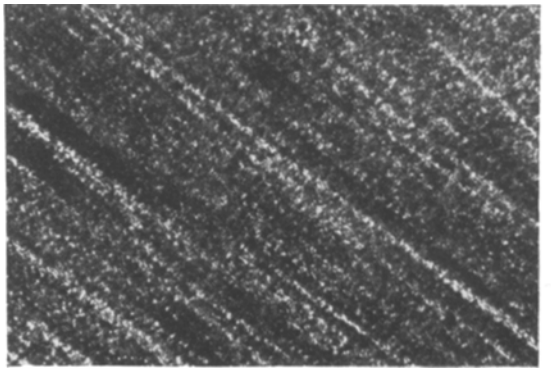

Figure 2 Composition II isothermally crystallized at 1100° C. β-$CaSiO_3$ fibres in a matrix of residual glass (× 500).

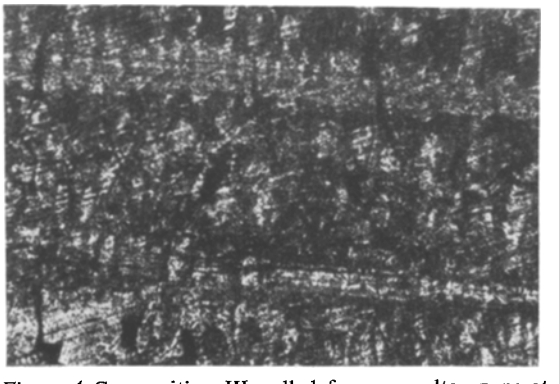

Figure 4 Composition III pulled from a molten zone at 30 μm sec^{-1} on a platinum spiral. α-$CaSiO_3$ dendrites in a matrix of $Ca_2ZnSi_2O_7$ and residual glass (× 500).

TABLE II Crystallization data for the materials which were investigated

Composition	Heat-treatment	Crystallization temperature (° C)	Primary phase	Crystallization mechanism	Fibre diameter (μm)	Matrix	Fibre orientation
I	Tile	1180	β-$CaSiO_3$	Spherulitic	60	$CaAl_2Si_2O_8$ and glass	Transverse
	Intracrucible	1180	β-$CaSiO_3$	Spherulitic	60	$CaAl_2Si_2O_8$ and glass	Longitudinal
II	Tile	1100	β-$CaSiO_3$	Spherulitic	5	Glass	Transverse and longitudinal
IIF	Tile	1100 Pulling speed $\mu m\,sec^{-1}$	β-$CaSiO_3$	Spherulitic	5	Glass	Random
III	Rod pulling	50	β-$CaSiO_3$	Spherulitic	2	$Ca_2ZnSi_2O_7$ and glass	Transverse and longitudinal
		30	β-$CaSiO_3$	Spherulitic	15		
			β-$CaSiO_3$	Dendritic	15		

parallel alignment when tiles of these glasses were isothermally crystallized at 1180 and 1100° C, respectively.

On devitrification at 1180° C, composition I gives fibres about 60 μm diameter of β-$CaSiO_3$ (a synthetic analogue of the mineral wellastonite, the low-temperature polymorph of calcium metasilicate) in a crystalline matrix of $CaAl_2Si_2O_8$ (a synthetic analogue of the mineral anorthite), together with a small amount of residual glass (see Fig. 1). After heat-treatment at 1100° C, composition II material consists of β-$CaSiO_3$ fibres approximately 5 μm diameter in a matrix of residual glass, as shown, in Fig. 2.

Maries and Rogers [13, 14] have described a novel technique for the directional devitrification of calcium metasilicate from a zone of molten glass, using glass composition III in Table I. The present authors have developed this technique to produce 1 cm diameter rods in which the primary fibrous crystals are aligned parallel to the rod axis [12, 15], and in which either β-$CaSiO_3$ fibres approximately 15 μm in diameter or dendritic "fibres" of α-$CaSiO_3$ (the high-temperature polymorph of calcium metasilicate) were formed in matrix of $Ca_2ZnSi_2O_7$ (a synthetic analogue of the mineral hardystonite) and residual glass, see Fig. 3 and 4.

The factors influencing the morphology of crystallization in these materials have been reviewed elsewhere by the present authors [15].

2. Experimental details

The full details of the production of these materials have been given in the recent paper by the authors [15]. The unidirectionally crystallized materials were fabricated by one of three methods, depending on the crystal growth rate of the composition used and on the dimensions of the specimens required (see Table II).

To produce "perpendicular" (P) or "transverse" (T) type rectangular prism specimens, in which the fibres are orientated at right angles to the long axis of the prism (see Fig. 5), tiles of glass were cast and whilst still at high temperature these were transferred to a muffle furnace and subjected to an isothermal heat-treatment. Crystallization was nucleated on the external surfaces and crystals grew orthotropically into the body of the tile from the two opposing larger area faces so as to meet at the centre. This technique was found to be suitable for compositions in which crystals grow at rates up to 5 $\mu m\,sec^{-1}$. In addition to composition II unidirectionally crystallized material, a tile of IIF internally nucleated material was prepared. This composition will produce nuclei at a relatively low temperature on which crystals can develop and grow when the ambient temperature is increased [16]. In this case the β-$CaSiO_3$ was

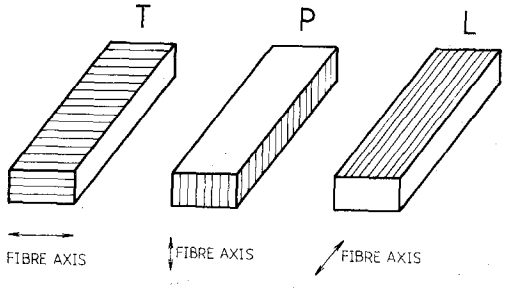

Figure 5 Rectangular prism test specimens with fibres orientated transversely (T), perpendicularly (P) or longitudinally (L).

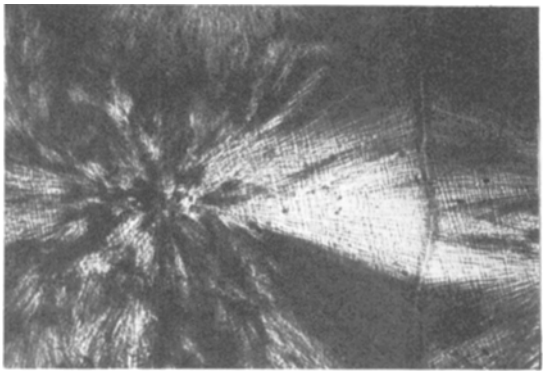

Figure 6 Devitrified composition IIF material, heat-treated at 750° C for 1 h to develop internal nuclei and then at 1100° C for $\frac{1}{2}$ h to allow the material to crystallize as spherulites from these nuclei (× 80).

produced in the form of true, freely developed spherulites (see Fig. 6), and this material was used to make specimens in which the fibres were in "random" orientation. The materials were cooled slowly after quenching below the crystallization region, so as to minimize thermal shock.

"Longitudinal" (L) type specimens, in which the fibre axis is aligned parallel to the long axis of the prisms (see Fig. 5), were produced by an intra-crucible isothermal heat-treatment technique for compositions in which the crystal growth rate does not exceed $2\,\mu m\,sec^{-1}$. In this the glass was melted in a fused alumina crucible and the glass-filled crucible was subsequently cooled and used as an *in situ* mould. The crystals nucleated on the crucible walls and grew radially into the glass, producing long, approximately parallel, fibrous crystals. For suitable compositions which crystallize at greater than about $10\,\mu m\,sec^{-1}$, the dynamic rod-pulling technique was employed. In this the molten glass was contained in a cylindrical platinum collar which was heated directly by an electric current. A nucleation agent could be dipped into the bottom of the melt and then pulled out at a constant rate, so that the glass rod produced crystallized unidirectionally down the temperature gradient below the collar. Composition III was used in this apparatus and at a pulling speed (equal to the crystal growth rate once a dynamic equilibrium is attained) of $30\,\mu m\,sec^{-1}$ two types of material could be produced. With a platinum wire spiral nucleation agent aligned dendritic α-$CaSiO_3$ crystals grew with the primary dendrite arms parallel to the pulling (rod) axis. When a β-$CaSiO_3$ seed crystal (a block of devitrified composition II) was used then β-$CaSiO_3$ fibres developed, the fibre axis being coincident with the rod axis. Therefore two types of material could be produced having identical chemical compositions and having undergone the same heat-treatment cycle (except for a slightly different crystallization temperature (Table II), but containing different phases in different morphologies.

The rectangular prism test specimens were prepared by sectioning the bulk materials in the relevant orientations using diamond impregnated slitting wheels. The tension faces of the beams used in the three-point bend tests were given a standardized abrasion treatment with a 600 grit diamond impregnated peripheral grinding wheel. Three-point bend tests were performed using a steel rig mounted on "Instron" testing machines. The rigs were fixed by coupling systems containing pin-joints or ball-bearings in order to eliminate any non-linearity in the apparatus, and were connected to the Instron cross-head and load cell in the reversing mode. The test specifications are given in Table III. The 20 mm span tests used rotatable tungsten carbide rollers to apply the load, but the smaller apparatus used for the 7 and 4 mm span tests employed hardened-steel knife-edges, coated with PTFE tape to eliminate any friction. The fracture surfaces obtained after breaking the specimens were observed using a scanning electron microscope.

An automatic recording dilatometer was used to measure the thermal expansion characteristics of the materials [17]. Specimens were prepared

TABLE III Specifications of the three-point bend tests used to measure molulus of rupture and interlamellar shear strength

Span ($\times 10^3$ m)	Specimen dimensions ($\times 10^3$ m)			Span : depth ratio	Cross-head speed ($\times 10^3$ m min^{-1})	Strain-rate ($\times 10^3$ min^{-1})
	length	breadth	width			
20	30	5 ± 0.25	2.5 ± 0.25	8:1	0.1	3.8
7	10	1.7 ± 0.2	0.9 ± 0.2	8:1	0.1	11.0
4	5	2.5 ± 0.2	1.0 ± 0.2	4:1	0.1	37.5

in the form of rectangular prisms approximately 5 mm by 5 mm in section and up to 15 mm in length. Examples from all the synthetic calcium metasilicate materials which had been mechanically tested were investigated, together with specimens of the original uncrystallized glasses and, in the case of composition II material, a glass of approximately the same composition as the inter-fibre residual glass (see Table I).

The fibre volume fractions were found by modal analysis [18]. Thin sections of the tested materials were prepared and were observed under transmitted light on a polarizing microscope to which a Swift point counting stage had been attached. The reliabilities of the percentages calculated were found using the chart devised by Van der Plas and Tobi [19].

The phases present in the crystallized material were identified from powder X-ray diffraction photographs taken using a Guinier asymmetric focusing camera.

3. Results

3.1. Microstructure of selected materials

3.1.1. Densities

Table IV gives the mean densities found from samples of each of the three compositions from which test specimens were prepared. The densities were measured by the standard displacement of water technique.

All the crystallized materials show a small decrease in density compared to the parent glass. The density of a glass-ceramic is an additive function of the densities of the various crystalline and glass phases present [6]. Porosity does not usually develop during the formation of internally nucleated glass-ceramics since the overall volume changes are very small and the final grain size is only about 1 μm. However, there is evidence from the fracture mechanism of the unidirectionally crystallized materials (see Section 4.2) that there are cracks running along the fibre/matrix interfaces, probably formed during cooling from the fabrication temperatures. In these fibrous structures the interfacial area is large and, therefore, even extremely narrow cracks may make significant contributions to the total volume of the material.

TABLE IV Densities of the glasses and the derived crystalline materials

Composition (see Table I)	Material	Mean density ($Mg\,m^{-3}$)
I	Glass	2.85
	Crystalline tile	2.78
	Crystalline intracrucible	2.75
II	Glass	2.75
	Crystalline tile	2.60
IIF	Glass	2.75
	Crystalline tile	2.61
III	Glass	2.97
	III 30β rod	2.85
	III 30α rod	2.93

The measured density of wollastonite is $2.88\,Mg\,m^{-3}$ (calculated density $2.96\,Mg\,m^{-3}$) and the measured density of pseudowollastonite is $2.91\,Mg\,m^{-3}$ (calculated density $2.90\,Mg\,m^{-3}$) [20]. As one of the calcium metasilicate modifications is the predominant phase in all the materials in Table IV, the density of the crystallized materials should have been of the order of $2.9\,Mg\,m^{-3}$.

3.1.2. Volume fractions of phases

Table V gives the results obtained from the modal analyses made on the crystallized materials. All the materials have a high fibre volume fraction, which is greater than that obtainable in rod morphology *in situ* composites [1].

Figs. 1 to 4 are high magnification optical micrographs of the I T, II T and L, III 30β and III 30α unidirectionally crystallized materials.

3.2. Thermal expansion characteristics

The thermal expansion coefficients quoted in Table VI were calculated from the results obtained from the automatic recording dilatometer, taking account of the various errors associated with this type of instrument [12], appendix I). In order to calibrate the dilatometer the thermal expansion coefficient of "spec-pure" silver was measured and calculated to be $20.35 \times 10^{-6}\,K^{-1}$ (20 to 650° C). This is within 1.5% of the tabulated value of $20.6 \times 10^{-6}\,K^{-1}$ (0 to 500° C) [21].

The thermal expansion anisotropy of wollastonite mineral was investigated for comparison [17]. Wollastonite has a triclinic crystal structure and forms orientated aggregates and is, therefore, likely to exhibit anisotropic thermal expansion [22], but tabulated values for the linear thermal expansion coefficient of wollastonite do not specify the orientation measured or the form of the temperature dependence. A sample of the

TABLE V Results of point counts performed on the devitrified materials.

Material	Phases (C = CaO, A O Al_2O_3, S = SiO_2, Z = ZnO)	Vol% of phase	2σ value %	Relative 2σ value (rel. %)
I				
Tile 3	β-CS fibres	62	± 3	5
	CaS_2 + α-CS	26	± 3	10
	Cracks + glass	12	± 2	16
I				
Tile 4	β-CS fibres	59	± 3	5
	CAS_2 + α-CS	33	± 2.5	8
	Cracks + glass	8	± 1.5	16
I				
Tile 6	β-CS fibres	52	± 2.5	5
	CAS_2 + α-CS	36	± 2.5	7
	Cracks + glass	12	± 2	16
I				
Intra-crucible	β-CS fibres	46	± 2	5
	CAS_2 + α-CS	42	± 2	6
	Cracks + glass	12	± 1.5	12
II				
Tile 2	β-CS fibres	62	± 3	4
	Glass	35	± 2.5	8
	Cracks	3	± 1	24
II				
Tile 4	β-CS fibres	64	± 3	5
	Glass	24	± 3	12
	Cracks	8	± 2	24
II				
Tile 5	β-CS fibres	66	± 3.5	5
	Glass	29	± 3.5	12
	Cracks	5	± 1.5	32
III 30β				
Rod	β-CS fibres	74	± 2.5	3
	C_2ZS_2 + glass	23	± 2.5	10
	Cracks	3	± 1	24
III 30α				
Rod	α-CS dendrites	67	± 3.5	6
	C_2ZS_2 + glass	31.5	± 3.5	12
	Cracks	1.5	± 1	40

mineral from Meldon, Devon (BM 1913, 253) in the form of an aggregate of parallel fibres was obtained from the British Museum (Natural History). Fig. 7 is a plot of mean percentage expansion versus temperature, measured both parallel to the fibre axis (L specimen) and perpendicular to the axis (T specimen). The L specimen shows a linear increase in dimension with temperature, i.e. there is an approximately constant expansion coefficient of the range 20 to 650° C. In the T specimen the rate of expansion increases with increasing temperature, indicating that the coefficient in this orientation rises from a value below the longitudinal coefficient at room temperature to one above it at 650° C, the expansion anisotropy of wollastonite reversing at 300° C.

The results of the dilatometric investigation of the compositions I, II and III, both original glasses and heat-treated materials, are given in Table VI. From this, and from the plots of mean percentage expansion versus temperature (Figs. 8 to 10), it was found that in the T specimens the expansion was dominated by the characteristics of the inter-fibre matrix, whereas in L specimens containing parallel fibres the linear expansion of β-$CaSiO_3$ in this orientation was evident in the measured values. However, in the composition I crystallized material, the expansion both in the T and L specimens was almost the same, which may have been due to the less exact alignment of the fibres in this material.

The percentage expansion versus temperature

TABLE VI Expansion coefficients calculated from the results of the dilatometric testing of both the glasses and the crystalline materials

Specimen	T(° C)	Expansion coefficient $20 \rightarrow T$° C
Wollastonite T	650	7.8
Wollastonite L	650	6.2
I glass	755	7.3
I T	650	6.2
I L	650	6.1
II glass	700	10.6
II R glass	600	10.5
II T	650	7.3
II L	520	6.1
II F	650	6.4
III glass	700	7.1
III 50 β T	650	4.6
III 30 β T	650	4.2
III 30 α T	650	5.0
III 50 β L	650	5.3
III 30 β L	650	5.8
III 30 α L	650	8.6

plots of the original glasses, and for the heat-treated materials which contain significant amounts of residual glass, show a slight change of slope at the glass transition temperature (T_g). For composition II crystallized material the composition of the residual glass (II R) could be calculated, knowing the volume percentage of calcium metasilicate from the results of the point counts (see Table I). It is shown in Fig. 9 that T_g for glass IIR corresponds to the T_g found for the crystallized materials.

The composition III specimens, prepared from materials produced by the rod-pulling technique, showed a decrease in percentage expansion with the pulling rate of the rod, i.e. with an increase in the amount of $Ca_2ZnSi_2O_7$ present as a secondary crystalline phase in the matrix between the fibres. The percentage expansion versus temperature plots of specimens prepared from a rod of composition III pulled at 10 μm sec^{-1} and which consisted of aligned, lath-shaped crystals of Ca_2ZnSiO_7 in residual glass are given in Fig. 11. This shows the mean percentage expansions calculated from results taken during both heating and cooling, and reveals considerable hysteresis in T and L specimens, together with very small positive or negative expansions. The III 30 α materials have larger expansion coefficients than the corresponding III 30 β specimens. This is in agreement with the reported expansion coefficient of α-$CaSiO_3$, 11.8×10^{-6} K^{-1} between 25 and 800° C [23], being much larger than those measured for β-$CaSiO_3$ (q.v.).

3.3 Mechanical properties

The moduli of rupture (R) were found from rectangular prism specimens machined from the selected materials so as to give three types of fibre orientation (see Fig. 5). The three-point bend test apparatus was calibrated using specimens prepared from "Purox" recrystallized alumina (Morganite Refractories Ltd) which has a reported modulus of rupture of 161 MN m^{-2} (16.4×10^6 kg m^{-2}). The results for this material, and all the other materials tested, are summarized in Table VII. Two spans were used to test the materials (since the rod materials were not available in sufficient quantities to produce the larger size specimens), but both tests had a span-to-depth ratio of 8:1 (see Table III). The moduli of rupture (R) were calculated from the loads at fracture (P), and the dimensions of the corresponding specimen, using the simple bending of cross-section, rectangular beams formula [24]

$$R = \frac{3PL}{2bd^2} \cdot g \ \text{N m}^{-2}$$

where L is the span of lower supports, b the specimen breadth, d the specimen depth, and g the acceleration due to gravity.

Only the results from those specimens which gave a load versus deflection curve showing a Hooke's law (linear) region were included. The specimens which did not display Hookean behaviour failed at very low loads since these were precracked beams (probably as a result of damage during machining) which fractured by crack extension at small applied stresses. The areas under the load versus deflection curves from these samples were used to obtain estimates of the works of fracture of the materials. Tattersall and Tappin [25] found that negligible energy loss occurs during catastrophic crack growth and, therefore, the area under a controlled fracture load versus deflection curve represents all the work done in the growth of the fracture crack and unavoidable damage directly related to the crack growth. The total work is divided by the nominal area of the two fracture faces to find the work of fracture. The values calculated are given in Table VII.

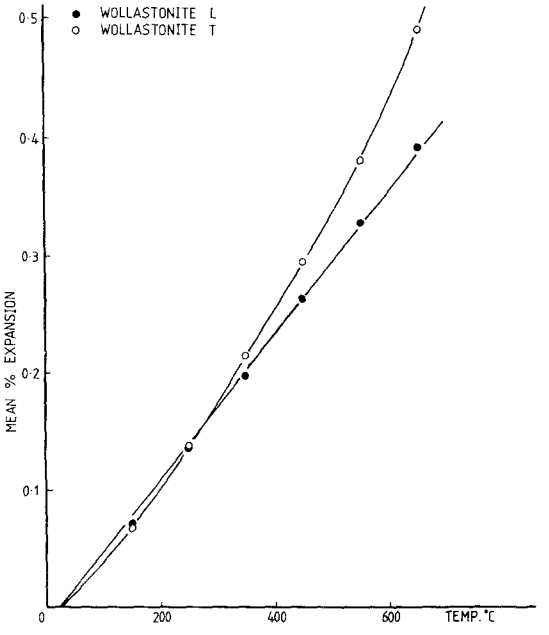

Figure 7 Percentage expansion versus temperature plots for wollastonite mineral with the fibre axis orientated parallel (L) or transverse (T) to the axis of the dilatometer.

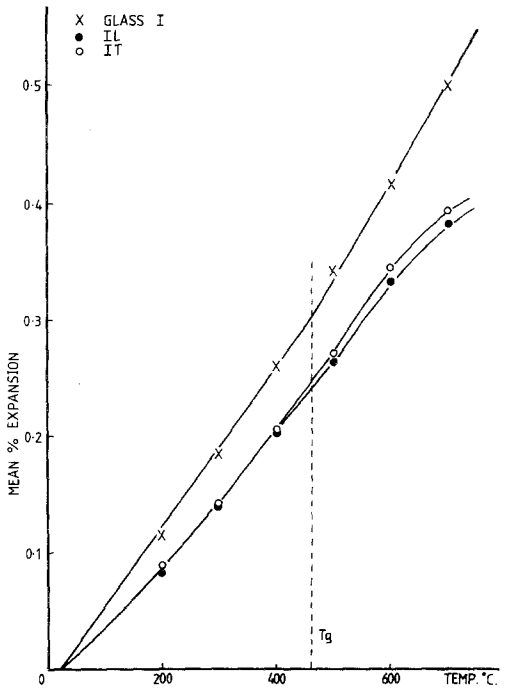

Figure 8 Percentage expansion versus temperature plots for composition I glass and devitrified material in L and T orientations.

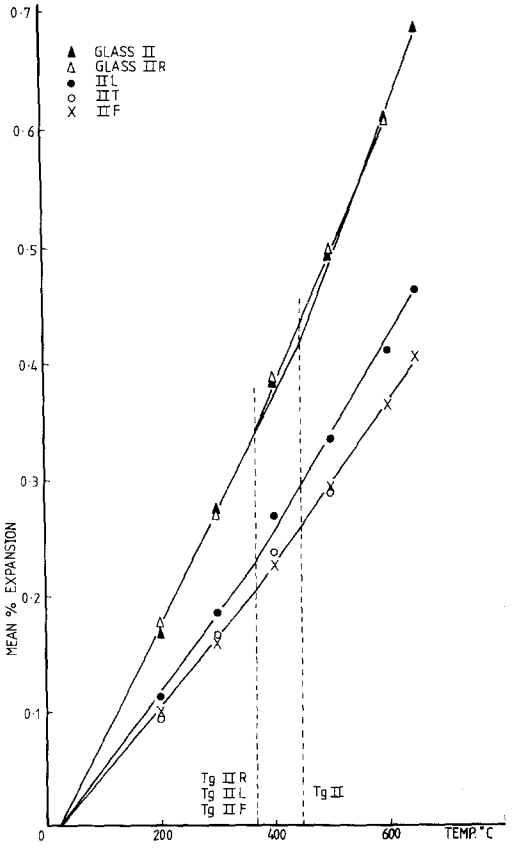

Figure 9 Percentage expansion versus temperature plots for composition II glass and devitrified material in L, T and random fibre (IIF) orientations, together with the calculated residual glass composition IIR.

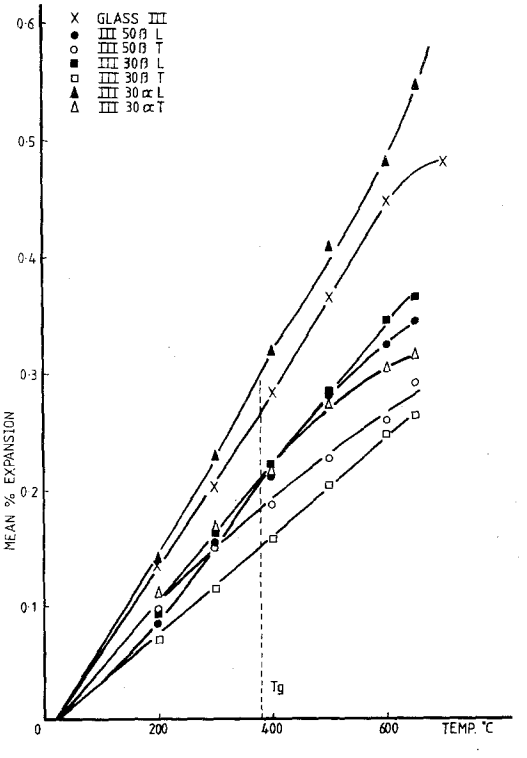

Figure 10 Percentage expansion versus temperature plots for composition III glass and devitrified materials in L and T orientations.

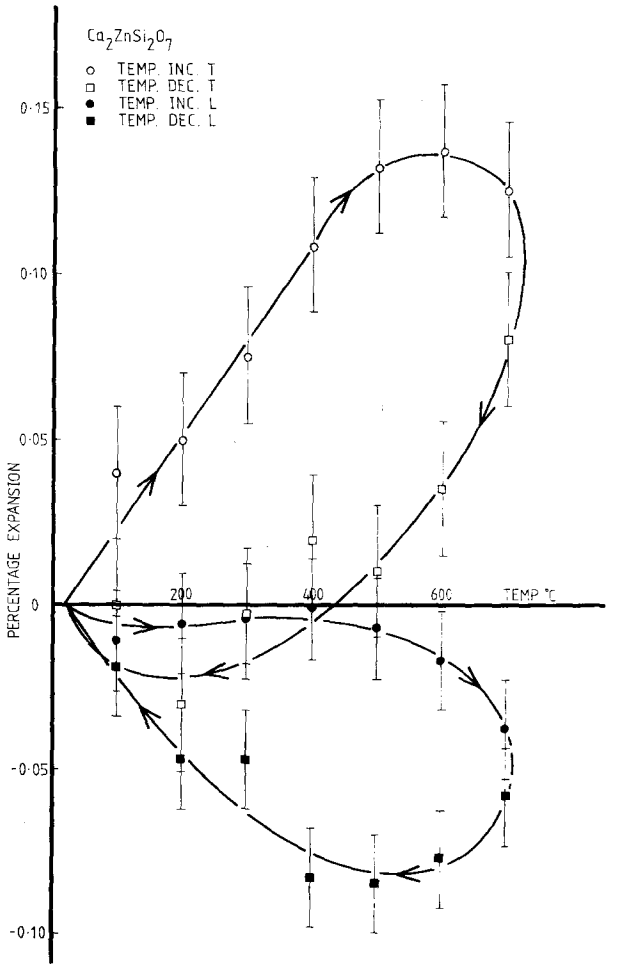

Figure 11 Percentage expansion versus temperature plots for $Ca_2ZnSi_2O_7$ phase material, produced from composition III glass by the rod-pulling technique at 10 μm sec^{-1}.

TABLE VII Results of the mechanical tests performed on the devritrified materials

Material	Fibre orientation	Test span ($\times 10^3$ m)	Number of results, n	Mean modulus of rupture, $\bar{R}$ (MN m^{-2})	Mean interlamellar shear strength $\bar{B}$ (MN m^{-2})	Standard deviation S	Coefficient of variance $S \times 100\%$ mean	Work of fracture (kJ m^{-2})
Purox alumina	–	20	11	177.8	–	23.5	13	–
Purox alumina	–	7	20	192.2	–	17.0	9	–
I tile 4	Perpendicular	20	7	11.1	–	3.7	33	0.01
I tile 6	Transverse	20	6	11.1	–	4.7	40	0.01
I intracrucible	Longitudinal	20	6	33.5	–	5.8	17	0.16
I tile 3	Longitudinal	4	45	–	6.4	1.8	28	–
II tile 2	Perpendicular	20	6	16.0	–	4.5	28	0.02
II tile 2	Transverse	20	7	11.8	–	4.5	38	0.02
II tile 4	Longitudinal	4	22	–	5.8	2.7	47	0.13
II tile 5	Longitudinal	4	18	–	5.8	2.9	49	0.13
IIF tile 1	Random	20	9	8.9	–	1.7	19	0.02
III 30β	Longitudinal	7	12	108.9	–	36.1	33	0.17
III 30β	Longitudinal	4	15	–	10.6	5.5	52	–
III 30α	Longitudinal	7	26	91.8	–	19.6	21	0.02
III 30α	Longitudinal	4	6	–	6.6	3.1	47	–

The interlaminar shear strengths (B) of the unidirectionally crystallized materials were found using short-beam three-point bend tests of span-to-depth ratio 4:1 on longitudinal-type specimens. The test specifications (see Table III were based on the work of Phillips *et al.* on carbon fibre-reinforced glass [26]. Only those results which corresponded to fracture surfaces showing some oblique character were used to calculate B values, i.e. where fracture had occurred at least partially by shear along planes parallel to the natural axis of the beam. The values of B were calculated using the standard formula [24]

$$B = \frac{3P}{4bd^3} \cdot g \,\mathrm{N\,m^{-2}}$$

and the mean results are listed in Table VII.

4. Discussion

4.1. Thermal expansion characteristics

4.1.1. Composition I

The thermal expansion coefficient of anorthite has been reported as $4.5 \times 10^{-6}\,\mathrm{K^{-1}}$ (100 to 200° C) [27]. A synthetic analogue of this mineral exists as a secondary phase in devitrified composition I. The magnitude of the expansion coefficient of the prepared specimens perpendicular to the unidirectional fibre axis could be estimated from a knowledge of the volume fraction and respective expansivities of the phases present. Using this approximation an expansion coefficient of $7 \times 10^{-6}\,\mathrm{K^{-1}}$ (20 to 650° C) is obtained for the crystalline composition I materials. The experimentally determined mean expansion coefficients for these materials increase from $4.7 \times 10^{-6}\,\mathrm{K^{-1}}$ at 100° C to $6.2 \times 10^{-6}\,\mathrm{K^{-1}}$ at 650° C, i.e. at 100° C the coefficient is close to that of the matrix phase only, and the coefficient is still lower than the estimated value at 650° C.

These results may be explained by considering the state of the fibre/matrix interfaces in this material, which was fabricated at nearly 1200° C and subsequently cooled to room temperature. At high temperatures the expansion coefficient of wollastonite is approaching twice that of anorthite, and therefore on cooling the fibre/matrix interface is put into tension and may fracture. With further cooling an open crack may form at the interface. Therefore, on reheating this material, initially the transverse expansion of the fibres only fills these cracks and the bulk transverse expansion measured corresponds to the matrix material only. As some of the cracks are closed the bulk expansion coefficient increases with temperature as the contribution from the relatively high expansion coefficient fibres increases. It is possible that not all the cracks were closed at 650° C. The devitrified material must contain a small amount of residual glass (from consideration of the compositions and proportions of the crystalline phases precipitated from the original glass), but since there is no indication of the material softening at 650° C, there can be only a small proportion present. This glass should have a high softening temperature from consideration of its estimated composition.

4.1.2. Composition II

The results obtained for crystallized composition II transverse specimens show the effect of a glass interfibre matrix. The percentage expansion versus temperature plots (Fig. 9) show a glass transition temperature (T_g) at about 370° C and the bulk material just starts to soften at 650° C. The glass made up with the same composition as the residual glass (glass IIR, see Table I) gave a T_g value at around the same temperature as that for the crystallized composition II materials, and softened at just above 600° C. The higher softening temperature of the crystallized material may be a result of the stiffening effect of the reinforcing fibres.

In these specimens the thermal expansion of the matrix, glass IIR, is $10.5 \times 10^{-6}\,\mathrm{K^{-1}}$ below T_g. This is greater than the transverse coefficient of the fibres. At high temperatures the matrix could flow and eliminate any stresses generated at the fibre/matrix interfaces during cooling from the fabrication temperature. In this case open cracks should not form at the fibre/matrix interfaces. The measured coefficients were found to correspond within 10% with the estimated transverse coefficient.

When the composition II crystallized materials were tested parallel to the fibre axis it was found to behave almost identically to the longitudinal wollastonite specimen. This shows that in this material the fibres are in good alignment and are continuous along the length of the dilatometer specimens. The glass matrix has a much higher expansivity than the β-$CaSiO_3$ fibres and, therefore, there may be open cracks in the matrix perpendicular to the fibre axis, produced whilst the material cooled from the fabrication temperature. This would mean that the matrix

expansion parallel to the fibre axis would be taken up in closing these cracks and, therefore, the externally measured matrix coefficient would be less than the true value. This may explain why the high expansion matrix does not dominate the expansion along the fibre axis.

4.1.3. Composition III

Four crystallized materials of this composition were investigated. III/50β consists of β-$CaSiO_3$ fibres in a matrix of glass together with a small amount of $Ca_2ZnSi_2O_7$ and was pulled from the hot collar at 50 $\mu m\,sec^{-1}$; III/30β which contains a larger proportion of $Ca_2ZnSi_2O_7$ in the glass matrix and was pulled at 30 $\mu m\,sec^{-1}$; III/30α, consisting of α-$CaSiO_3$ dendrites in a matrix of glass and $Ca_2ZnSi_2O_7$, and $Ca_2ZnSi_2O_7$ tabular crystals only, pulled at 10 $\mu m\,sec^{-1}$.

The transverse fibre specimens all have low overall percentage expansions. This is due to the very low expansion coefficient and the hysteresis displayed by the interfibre $Ca_2ZnSi_2O_7$ phase (see Fig. 11). Transverse specimens of $Ca_2ZnSi_2O_7$ showed a small percentage expansion during heating but on cooling a rapid contraction produced a hysteresis loop and resulted in negative expansion, i.e. an overall contraction. The longitudinal specimens show a very small contraction on heating and again on cooling rapid additional contraction produced a hysteresis loop.

A negative expansion coefficient can be produced in open, network types of silicate crystal structures [28]. However, this would not explain the hysteresis effect, which is similar to the expansion characteristics of zirconia–yttria solid solutions [29, 30]. The hysteresis in that system is due to the tetragonal to monoclinic polymorphic change in the zirconia structure which occurs during heating and involves a large change in volume. Since the solid solution is not completely homogeneous, and the amount of yttria present controls the transformation temperature, the transformation is spread over a range of temperatures. Hardystonite, the mineral analogue of $Ca_2ZnSi_2O_7$, has the melilite structure which is known to be capable of existing as a wide range of solid solutions [31]. The melilites have no known polymorphs [32], but there is some evidence of a volume change resulting from a structural inversion (the "peg structure" found in some melilite minerals). The $Ca_2ZnSi_2O_7$ must contain excess calcium ions in solution. This was shown by a comparison of the powder X-ray diffraction results for this phase and those obtained from $Ca_2ZnSi_2O_7$ which grew in association with α or β-$CaSiO_3$, i.e. the d-spacings for the $Ca_2ZnSi_2O_7$ only material were shifted to larger values by approximately 10%.

The transverse thermal behaviour of the IIIα and β materials can be related to the amount of $Ca_2ZnSi_2O_7$ present in each. III/50β contains only a small amount of this secondary crystalline phase in the matrix and, therefore, although the overall expansion coefficient is reduced, this material does not give a hysteresis loop on cooling. The III/30α and β materials both include more $Ca_2ZnSi_2O_7$ and these give hysteresis effects on thermal cycling, in addition to reduced expansion coefficients.

The results for the III/50β and III/30β longitudinal specimens are very similar, both showing the constant expansion coefficient characteristic of wollastonite parallel to the fibre axis. The coefficients are lower than that found for longitudinal wollastonite, which may be due to the presence of the low expansion $Ca_2ZnSi_2O_7$ phase, nucleated at the fibre/matrix interfaces, inhibiting the free expansion of the fibres. The β-$CaSiO_3$ fibres in the III/50β and III/30β must be in good parallel alignment, and be continuous, to dominate the expansion characteristics.

The III/30α longitudinal specimens do not show any evidence of significant hysteresis. There must be a relatively large amount of residual glass left between the dendritic arms in this material as a T_g of 350° C was found, although there was no indication of dilatometric softening up to 650° C. The expansion coefficient is again lower than the reported value for α-$CaSiO_3$, ($11.8 \times 10^{-6}\ K^{-1}$, 25 to 800° C, [23] but it does increase gradually with temperature.

4.2. Mechanical properties

4.2.1. Materials containing β-$CaSiO_3$ fibres

The mechanical properties of these materials may be interpreted by considering them as unidirectional fibre-reinforced composites. The modulus of rupture (R) results show the influence of fibre orientation on the measured strengths. Unidirectional fibre composites under the action of a tensile stress applied at an angle θ to the fibre axis generally fracture by one of three mechanisms [33].

(1) When θ is small failure occurs in the plane

perpendicular to the fibre axis and is due to tensile failure of the fibres.

(2) At values of θ between 5 and about 45°, failure is by shear in the direction of the fibres on a plane parallel with the fibres.

(3) At larger values of θ the fibre/matrix interface fails in tension. The fracture mode that requires the lowest stress occurs, and when this is calculated it is found that the fracture stress decreases rapidly as θ increases.

The mean R results for the composition IP, T and L specimens are all relatively low compared with glass-ceramic materials, typical bend strengths of which are around $150\,MN\,m^{-2}$, and are also lower than the bend strength of glass, about $100\,MN\,m^{-2}$ [34]. The value obtained for the L type specimens is approximately three times that for the P or T types (see Table VII). In the L orientation, failure occurs by a combination of interfibrillar (interface) separation and fracture across fibre bundles, and the fracture stress is strongly dependent on the exact angle between the fibre axis and the tensile axis (direction of maximum stress). The 10° misorientation of the fibres inherent in this particular material reduces the value of R to about 40% of the maximum value [33].

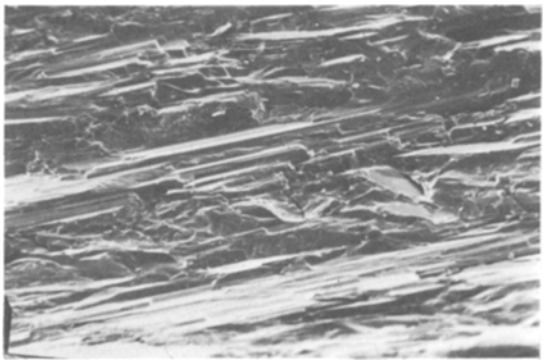

Figure 12 SEM micrograph of the fracture surface of a composition I devitrified material tested in three-point bend transverse to the β-$CaSiO_3$ fibre axis (× 250).

Fig. 12 is an SEM micrograph of the fracture surface from a IT beam. Fracture occurred between the fibres, the tensile stresses having fractured the weak fibre/matrix interfaces, leaving the fibres intact. There appears to be a degree of orientation of the fibres normal to the fibre axis. Some areas of matrix can be seen.

Fig. 13 is an SEM micrograph of the strongest IIP specimen. This shows that failure occurred by interfibrillar fracture together with some shearing of the fibre layers. This material consists of continuous β-$CaSiO_3$ fibres in a matrix of residual glass, the fibre volume fraction being about 0.6. Although in composition II material the differential thermal expansion is not such that open cracks are formed at the fibre/matrix interface during cooling from the crystallization temperature (see Section 4.1.2), there may be stress-raisers such as crystal facets and inperfections present at the interface which could give a loss of crystal/glass coherence at low applied tensile stresses (possibly during fabrication of the beams). If the interfacial tensile strength is zero, the P or T orientation strength of the material will be that of an equivalent volume of glass containing cylindrical voids [26]. A typical value of R for glass is $100\,MN\,m^{-2}$ and, therefore, using the law of mixtures and allowing for the 0.6 volume fraction of fibres the composite strength is reduced to $40\,MN\,m^{-2}$. The stress-concentrating effect of circular cross-section cylinder is a factor of 3 [26], and this reduces the theoretical P or T composite strength to $13\,MN\,m^{-2}$. This is in good agreement with both the P and T results ob-

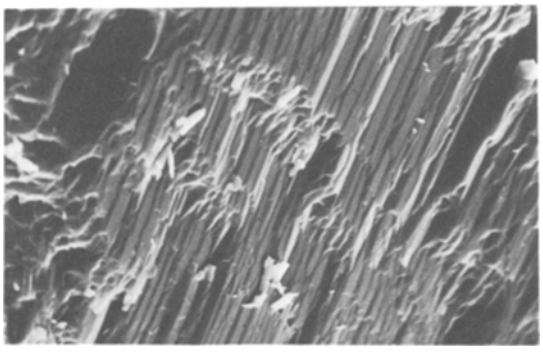

Figure 13 SEM micrograph of the fracture surface of a composition II devitrified material tested in three-point bend perpendicular to the β-$CaSiO_3$ fibre axis (× 1000).

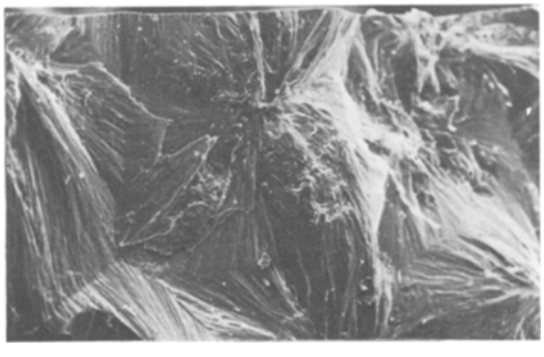

Figure 14 SEM micrograph of the fracture surface of a composition IIF internally nucleated devitrified material tested in three-point bend (× 50).

tained from the composition II materials (see Table VII.

In Fig. 13, the approximately square cross-section of the fibres can be seen, and the orientated packing of the fibres normal to the fibre axis is also clearly shown.

The mean R value found for the IIF random fibre orientation material is somewhat lower than those for IIP or T, but the coefficient of variance is much lower. Fig. 14 is a SEM micrograph of the fracture surface of a IIF beam. The fracture path passes through the spherulite centres, which can be seen standing proud on the fracture surface, and not along the boundaries between the impinging spherulites. There was no evidence found of any cracks forming where the crystal growth fronts meet. It therefore appears that fracture again occurs along the fibre/glass matrix interfaces inside the spherulites. The relatively low variability of the IIF moduli may be a reflection of the random fibre orientation, since any crack or flaw introduced during machining beams from the material is limited as the interfibrillar cracks are deflected by fibres in other orientations. In a unidirectionally crystallized material there are crack paths which could extend right across one dimension of a beam.

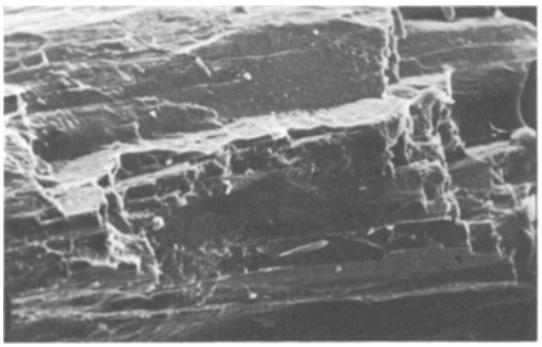

Figure 15 SEM micrograph of the fracture of a composition III β-$CaSiO_3$ phase directionally devitrified material, tested in a short-beam test to determine the interlaminar shear strength (× 250).

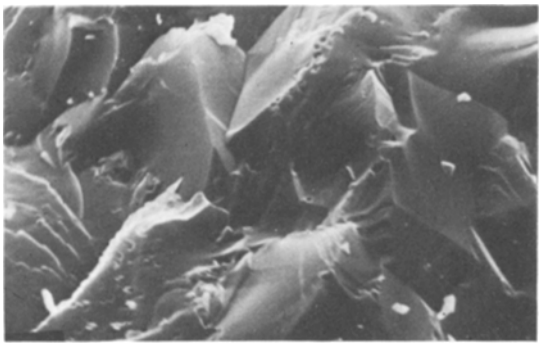

Figure 16 SEM micrograph of the fracture surface of a composition III α-$CaSiO_3$ phase directionally devitrified material tested in three-point bend parallel to the primary dendrite spine axis (× 2500).

The mean R value for the III 30 β L specimens is about three times greater than that found for the I L beams. This is a result of the better colinear alignment of the fibres in this material, i.e. the fibre orientation varies by only five degrees, which means that the measured modulus was at least 70% of the maximum. The shorter span three-point bend tests also give higher moduli than the 20 mm span tests, as is shown by the results for the alumina specimens. The coefficient of variance for the tests on III 30 βL is high, which may be due to only a few specimens being cut from each rod (a maximum of four). Fracture surfaces consist of large fracture steps, failure being primarily trans-fibrillar, but with deflected cracks running between the groups of fibres which nucleated from the same site and which have related (0 1 0) plane orientations. The fracture steps are produced when a trans-fibrillar crack is deflected by one of these stronger fibre groups.

In this material, the matrix thermal expansion is less than that of the β-$CaSiO_3$ fibres and this will give weak fibre/matrix interfaces, although the large proportion of glass in the matrix would relieve stresses at temperatures above T_g. Also the fine fibre diameter (less than 15 μm) will lessen the differential in dimensions so that the tensile stress across the fibre/matrix interface may not exceed the fracture stress and open cracks will not develop. This would also account for the greater strength of the III βL specimens compared with the Iβ L specimens, both for R and B, the inter-lamellar shear strength. IIIβ specimens failed with very oblique fracture when subjected to short beam tests to give values of B. This indicates that they failed almost totally in shear. Fig. 15 shows a typical fracture surface and from that it can be seen that fracture is primarily along the fibre/matrix interface. The trans-fibrillar fracture gives irregular non-planar fracture steps so some cracks propagate through fibre bundles and others through a single fibre. This behaviour is intermediate between the type I material, in which the cracks between the fibres and matrix deflect the fracture path so that single fibre fracture steps result, and the type II in which large fracture steps are formed across groups of fibres having related

(0 1 0) plane orientations. The microstructure of the III 30β material is also intermediate between these materials, i.e. fibres of about 15 μm diameter and a matrix consisting of a mixture of glass and crystals.

4.2.1. Material containing α-$CaSiO_3$ dendrites

The mean R value found for the III 30 α L specimens is similar to that of the III 30 β L specimens (see Table VII. The fracture surface of a typical III 30α L beam is shown in Fig. 16. This is a close-up of the uniform surface and does not show any fracture steps as were found for the III 30β L material. In the SEM micrograph it would appear that trans-dendrite failure has occurred with no "fibre pull-out". This implies that there are strong dendrite/matrix interfaces in this material. These strong interfaces may be due to the secondary dendrite arms which "key" the dendrite into the matrix in manner similar to the mechanical bond produced by growing whiskers on the surface of carbon fibres prior to their incorporation into a resin matrix [35].

The fracture surface for III 30α specimens tested by short beam tests to find B values are not as oblique as those of III 30β tested in the mode. Fracture seemed to have been mainly through the matrix, only a few dendritic arms penetrating the surface. This is a consequence of the relatively strong dendrite/matrix interfaces. It is, therefore, surprising that the interlaminar shear strength found for III 30α is similar to that of the composition I, weak interface material (see Table VII. The very large scatter associated with these results, due to results from pre-cracked specimens which failed in tension being included in the calculated mean, makes it possible that the true mean B value for the dendritic material is higher than that found.

4.2.3. Work of fracture

For the determinations of the work of fracture of the I, II and III materials the pre-cracked specimens, rejected for strength measurements, were used. The results obtained are given in Table VII. Those for the transverse, perpendicular or random fibrous specimens are an order of magnitude lower than those for the longitudinal fibrous specimens. This is a result of crack deflection due to the weak interfaces in these materials. When a crack is propagating under stress in addition to the stress concentration tending to open the crack further in its own plane, there are also subsidiary stresses which tend to open cracks on planes normal to the plane of the crack. Therefore, if there are planes of weakness parallel to the tensile stress axis, then cracks propagating normal to this stress could be deflected [36]. Energy is expended in creating new surfaces and in increasing the length of the fracture path and thus the work of fracture is increased.

The transverse, perpendicular and random β-$CaSiO_3$ fibre specimens, and the material containing α-$CaSiO_3$ dendrites in any of the orientations, do not have weak interfaces normal to the tensile stress axis and, therefore, there is no increase in the work of fracture, i.e. it is the same order of magnitude as that found for commercial alumina ceramics [25]. However, the work of fracture for the longitudinal β-$CaSiO_3$ fibre specimens is increased by an order of magnitude. It is slightly higher for composition I and III in which the matrix contains a proportion of a secondary crystalline phase, and which should contain weaker interfaces than the fibre/glass matrix composition II materials (see Section 4.1).

5. Conclusions

5.1. Thermal expansion

The thermal expansion characteristics parallel and perpendicular to the fibre axis were determined for natural wollastonite (calcium metasilicate) mineral. The longitudinal and transverse expansions were also found for the synthetic materials. It was found that, generally, the expansion characteristics parallel to the fibre axis were dominated by the expansion of the fibres, whereas perpendicular to the fibres the interfibre materials dominated the measured expansions. Materials containing about 30% residual glass showed a glass transition temperature when tested transverse to the fibre axis. Rod-pulled materials containing $Ca_2ZnSi_2O_7$ as a secondary crystalline phase gave a hysteresis effect in the thermal expansion/contraction measured transverse to the fibre axis. This is possibly due to a previously unreported, reversible phase change in this secondary crystallization, interfibre, phase.

5.2. Mechanical properties

The mechanical properties of the unidirectionally crystallized specimens show that these materials can be treated as unidirectional fibre-reinforced

ceramic–matrix composites. It was found that the strengths of the materials were generally low, due to the damaging thermal shock effect of the differential expansion between the fibres and matrix. However, the strength parallel to the fibre axis was far greater than that perpendicular to the fibres, agreeing with the theories for composite materials. The strength results were similar for materials with a glass or crystalline, inter-fibre matrix, and SEM micrographs revealed that in both cases the fracture paths were along the fibre/matrix interfaces. Comparing the transverse strength of a glass matrix material (IIβ) to the calculated transverse strength of a glass matrix composite showed that the fibre/matrix interfaces have zero tensile strength.

The dendritic material tested behaved more like a homogeneous brittle solid since it contains strong dendrite/matrix interfaces due to the keying effect of the secondary dendrite arms.

The work of fracture results revealed an order of magnitude increase for materials tested so that cracks were deflected along weak fibre/matrix interfaces, i.e. for the materials containing β-$CaSiO_3$ fibres parallel to the tensile axis.

Acknowledgements

Dr R.M. Weston, now Dr (Mrs) R.M. Boff was supported during the course of this work by an S.R.C. Research Studentship. The authors wish to thank Dr A. Maries for many useful discussions, and Mr H. Haddow for assistance with the mechanical tests performed.

References

1. J. D. LIVINGSTON, *Mater. Sci. Eng.* 7 (1971) 61.
2. G. J. DAVIES, "Directionally-Grown Metallic Composties", Inst. Metallurgists Spring Meeting (1973) Series 3, no. 1.
3. F. L. KENNARD, R. C. BRADT and V. S. STUBICAN, *J. Amer. Ceram. Soc.* 57 (1974) 428.
4. F. M. A. CARPAY and W. A. CENSE, *Nature Phys. Sci.* 241 (1973) 19.
5. *Idem, Scripta Met.* 8 (1974) 11.
6. P. W. McMILLAN, "Glass Ceramics" (Academic Press, London, 1964).
7. M. TASHIRO, T. KOKUBO, S. ITO and M. ARIOKA, *Bull. Inst. Chem. Res. Kyoto Univ.* 53 (1975) 471.
8. K. H. G. ASHBEE, *Nature* 252 (1974) 569.
9. D. I. ATKINSON and P. W. McMILLAN, *J. Mater. Sci.* 10 (1975) 2012.
10. J. WILLIAMSON, A. J. TIPPLE and P. S. ROGERS, *ibid.* 4 (1969) 1069.
11. J. WILLIAMSON and P. S. ROGERS, *Verres Réfract.* 26 (1972) 53.
12. R. M. WESTON, Ph.D. thesis, University of London (1977).
13. A. MARIES and P. S. ROGERS, *Nature* 252 (1975) 401.
14. *Idem, J. Mater. Sci.* 13 (1978) 2119.
15. R. M. WESTON and P. S. ROGERS, *Mineral Mag.* 42 (1978) 325.
16. S. P. MUKHERJEE and P. S. ROGERS, *Phys. Chem. Glasses* 8 (1967) 81.
17. R. M. WESTON and P. S. ROGERS, *Mineral. Mag.* 40 (1976) 649.
18. F. CHAYES, "Petrographic Modal Analysis" (Wiley, New York, 1956).
19. L. VAN DER PLAS and A. C. TOBI, *Amer. J. Sci.* 263 (1965) 87.
20. L. HELLER and H. F. W. TAYLOR, "Crystallographic Data for the Calcium Silicates" (H.M.S.O., London, 1956).
21. B. A. ROGERS, I. C. SCHOONER and L. JORDEN, "Silver: Its Properties and Industrial Uses" (National Bureau of Standards, Washington, 1936) Circular C412.
22. G. BAYER, *Proc. Brit. Ceram. Soc.* 22 (1973) 39.
23. R. W. ANDREWS, "Wollastonite" (Inst. of Geological Sciences, H.M.S.O., London, 1970).
24. P. P. BENHAM, "Elementary Mechanics of Solids" (Pergamon Press, Oxford 1965).
25. H. G. TATTERSALL and G. TAPPIN, *J. Mater. Sci.* 1 (1966) 296.
26. D. C. PHILLIPS, R. A. J. SAMBELL and D. H. BOWEN, *ibid* 7 (1972) 1454.
27. R. H. STUTZMAN, J. R. SALVAGGI and H. P. KIRCHNER, "An Investigation of the Theoretical and Practical Aspects of the Thermal Expansion of Ceramic Materials" (U.S. Dept. of Commerce, Office of Technical Services, Washington, 1959).
28. H. D. MEGAW, *Mater. Res. Bull.* 6 (1971) 1007.
29. P. DUWEZ, F. H. BROWN and F. ODELL, *J. Electrochem. Soc.* 98 (1951) 356.
30. E. RYSHKEWITCH, "Oxide Ceramics, Physical Chemistry and Technology" (Academic Press, New York and London, 1060).
31. W. A. DEER, R. A. HOWIE and J. ZUSSMANN, "An Introduction to the Rock Forming Minerals" (Longmans, London, 1969).
32. H. S. YODER, *Fortshr. Miner.* 50 (1973) 140.
33. G. KITTEL, "Introduction to Solid State Physics", 4th Edn. (Wiley, New York, 1971).
34. J. W. DONALD and P.W. McMILLAN, *J. Mater. Sci.* 11 (1976) 949.
35. J. C. GOAN and S. P. PROSEN, "Interfacial Bonding in Graphite Fibre–Resin Composites" (ASTM STP 452, Washington, 1969) p. 107.
36. G. A. COOPER and A. KELLY, "Role of Interfaces in the Fracture of Fibre-Composite Materials", *ibid.*, p. 90.

Received 20 July and accepted 20 September 1978.